JOURNAL OF GEOPHYSICAL RESEARCH, VOL. 91, NO. B9, PAGES 9517-9532, AUGUST 10, 1986

THREE-DIMENSIONAL P AND S WAVE VELOCITY STRUCTURES OF SOUTHERN PERU AND THEIR TECTONIC IMPLICATIONS

Paul S. Cunningham[1] and Steven W. Roecker[2]

Department of Earth, Atmospheric, and Planetary Sciences,
Massachusetts Institute of Technology, Cambridge

Denis Hatzfeld

Laboratoire de Geophysique Interne
Institut de Recherches Interdisciplinaires de Geologie et de Mecanique
L'Universite Scientifique et Medicale de Grenoble, France

Abstract. In 1981 an 18-station regional array was operated in southern Peru above the area where the dip of the subducted Nazca plate changes from virtually horizontal in the northwest to about 30° in the southeast. Arrival times of compressional (P) and shear (S) waves from microearthquakes recorded by this array are used in this paper to investigate the three-dimensional velocity structure of the crust and upper mantle in the region between the coast and the Cordillera Occidental. The results suggest a crustal thickness of about 40 km beneath the coast, increasing to about 70 km beneath the Cordillera Occidental. This change in thickness occurs abruptly in the northwest but is gradual in the southeast. The inverse correlation between the dip of the Moho and the dip of the slab suggests a broad-scale, causal relation between the two. At the same time, free-air gravity anomalies suggest that the steepening of the Moho in the northwest may occur only in the region under the array. Because the crust is thicker in the southeast than originally surmised, a suite of earthquakes previously thought to occur in the mantle now appears to be confined to the crust. The association of these earthquakes with a shallow dipping Moho is suggestive of ongoing crustal deformation to the west of the Andes. However, other seismological and geological observations make the role of these earthquakes in crustal deformation unclear. S wave velocities in the mantle between 70- and 130-km depth above the 30° dipping slab are low, suggesting the presence of partially melted asthenosphere that may be responsible for the magmatic activity observed in southern Peru.

Introduction

The term "Andean margin" was introduced to define a tectonic environment in which a mountain belt is formed as a result of the subduction of oceanic lithosphere beneath a continent [Dewey and Bird, 1970; James, 1971]. An Andean margin is characterized by a voluminous magmatic arc bounded on one side by a trench and on the other by a fold and thrust belt, and is presumed to describe an early developmental stage of some ancient orogenic belts, such as that in western North America [Burchfiel and Davis, 1972, 1975; Hamilton, 1969]. As our knowledge of such margins increases, however, it has become evident that the generic term, Andean margin, embraces a broad spectrum of deformation styles, both in the type example of the Andes and in its earlier analogs. For example, the broad zone of deformation that exists in the Pampean ranges of Argentina with faults that extend into the crystalline basement contrasts with the thin-skin tectonic style in the Paleozoic sedimentary cover of Bolivia [Jordan et al., 1983]. Similarly, in western North America, the broad zone of deformation with faults extending into the basement in the Laramide of the western United States [Burchfiel and Davis, 1972, 1975; Sales, 1968; Stearns, 1978] contrasts with the thin-skinned fold and thrust belt of western Canada [Balley et al., 1966; Price and Mountjoy, 1970]. Therefore if one wishes to understand the mechanics of deformation in ancient Andean margins, it is imperative to study modern examples in greater detail.

Information about the mechanics of deformation in an area may be derived from determinations of the elastic wave velocity structure at depth. Changes in the dimensions or relative locations of various structures may be reflected in spatial variations of elastic parameters that give rise to variations in seismic wave velocity. In this paper we discuss the results of an inversion of arrival times of waves from locally recorded earthquakes for compressional (P) and shear (S) wave velocity structures in the crust and upper mantle of the central Andes. The inversion uses data from an array that was operated for 6 weeks in southern Peru, recording events from the trench to the western edge of the Altiplano and to depths of 200 km.

Tectonic Overview

The Andes mountain system extends continuously from about 5°S to 40°S along the western edge of the South American continent. Southern Peru, the area of interest in this paper, is within that part of the system commonly referred to as the "central Andes." Morphologically, the central Andes can be divided into five principal units (Figure 1): (1) the coastal plains, (2) the Cordillera Occidental, (3) the Altiplano, (4) the

[1]Now at Standard Oil Production Co., Dallas, Texas.

[2]Now at Department of Geology, Rensselaer Polytechnic Institute, Troy, New York.

Paper number 5B5873.
0148-0227/86/005B-5873$05.00

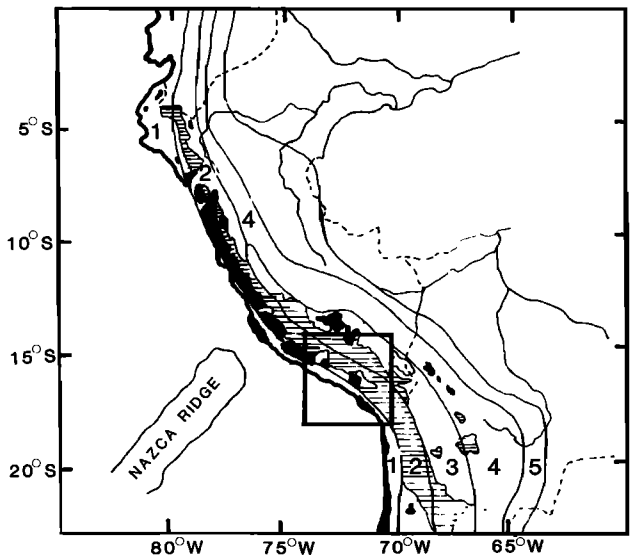

Fig. 1. Physiographic provinces of the Andes of Peru and northern Bolivia: (1) coastal plains, (2) Cordillera Occidental, (3) Altiplano, (4) Cordillera Oriental, and (5) sub-Andean zone. Shaded areas indicate plutonic bodies, and hatched areas the volcanic rock cover. Insert shows location of regional seismic array operated during 1981 [adapted from Dalmayrac et al., 1980].

Cordillera Oriental, and (5) the sub-Andes. In southern Peru the coastal plains are composed of the Arequipa block, a Precambrian massif containing rocks as old as 1.8 to 2.0 b.y. [Cobbing et al., 1977; Dalmayrac et al., 1977]. The Arequipa block is exposed near the coast and is covered by Quaternary and Tertiary sediments inland. The Cordillera Occidental is composed of volcanic and plutonic rocks of Mesozoic and Cenozoic age and shallow marine deposits of Mesozoic age. The main structural entity in the Cordillera Occidental is the Coastal Batholith, extending from about 6°S to 16°S and composed of gabbroic and syenogranitic plutons emplaced episodically from 100 to 30 m.y. ago [Cobbing and Pitcher, 1972; Cobbing et al., 1977; Pitcher, 1975]. Cenozoic volcanic rocks and Neogene ignimbrites are widespread in the Cordillera Occidental [Dalmayrac et al., 1980], the youngest of which indicate an abrupt end to volcanic activity in the north some 5 m.y. ago [Nobel and McGee, 1977]. A subhorizontal east directed thrust fault with a minimum displacement of 15 km marks at least part of the boundary between the Arequipa massif and the Cordillera Occidental [Vicente et al., 1979].

East of the Cordillera Occidental is the Altiplano, a plateau at 3000-m elevation that reaches a maximum width of 200 km near Lake Titicaca (Figure 1). Much of the Altiplano in southern Peru is covered by a thick sequence of continental molasse deposited in the Oligocene and Miocene [Newell, 1949] and, in contrast to the regions to the north, is only mildly deformed. The Altiplano is bounded to the east by the Cordillera Oriental, which is composed of Precambrian crystalline rock and Paleozoic plutonic and shallow marine and continental sedimentary rocks. The Precambrian rocks are weakly to strongly foliated and locally reach amphibolite to granulite grade. The Paleozoic rocks are generally unmetamorphosed to weakly metamorphosed. The deformation of these rocks has been attributed to a middle to late Paleozoic ("Hercynian") event [Dalmayrac et al., 1980; Megard, 1978].

The sub-Andean zone is a belt of folded sedimentary rocks lying between the Cordillera Oriental and the Brazilian shield. The boundary with the Cordillera Oriental is formed by a zone of west dipping thrust faults [Ham and Herrera, 1963]. The shallow water and continental sedimentary rocks of the sub-Andes were deposited intermittently from Paleozoic to Pliocene time and may reach a thickness of 10 km [Audebaud et al., 1973]. Deformation in the sub-Andes is difficult to date, but the age and intensity of deformation are typically shown to decrease steadily to the east [Dalmayrac et al., 1980]. Most of the large intraplate earthquakes in South America occur in the sub-Andes [Stauder, 1975; Suarez et al., 1983], indicating that it is a region of active and substantial crustal deformation.

The South American plate is bounded to the west by the Peru-Chile trench, along which the Nazca plate is subducting. Using teleseismically located hypocenters [Barazangi and Isacks, 1976, 1979], the subducted Nazca plate may be subdivided along strike into five distinct segments, each of which has a uniform dip. The segmented nature of the subducted slab may be intimately related with variations in tectonics observed at the surface [Barazangi and Isacks, 1976, 1979; Jordan et al., 1983] such as the cessation of volcanic activity in the north and the occurrence of intracrustal seismicity in the east. Likewise, the segmentation of the zone may result from the interaction of various topographic features on the Nazca plate, such as the Nazca and Juan Fernandez ridges, with the trench.

The area discussed in this paper is located above and south of one of the regions where the dip of the slab changes from nearly horizontal in the north to a more "normal" dip of 30° in the south (Figure 1). Despite the sudden change in dip, the slab appears to be continuous in this region [Hasegawa and Sacks, 1981; Grange et al., 1984], with the contortion in the slab being parallel to the direction of convergence [Grange et al., 1984].

Data and Preliminary Analysis

The data used in determining the three-dimensional P and S wave velocity structures of southern Peru are the arrival times of waves from earthquakes recorded by a temporary regional array (Figure 2). The array was operated during the summer of 1981 and was composed of 15 portable and three permanent stations. The permanent stations included the World Wide Standardized Seismograph Network (WWSSN) station ARE located near Arequipa and two others (ONG and AYE) installed by the Department of Terrestrial Magnetism (DTM) of the Carnegie Institute in Washington. (All three of these stations were maintained by the Instituto Geofisico at

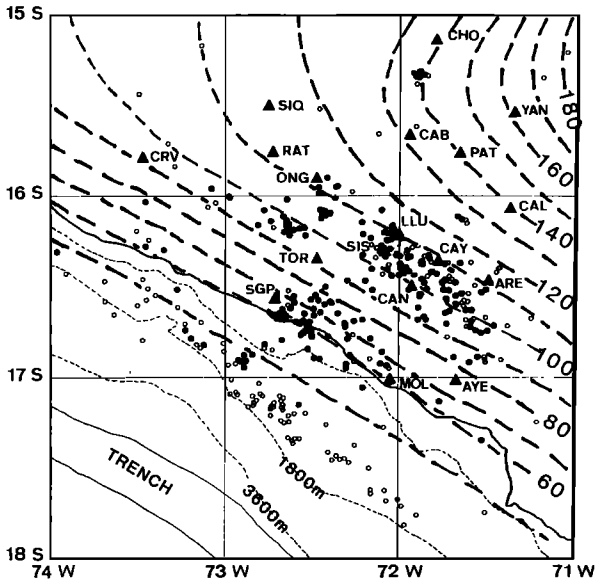

Fig. 2. Locations of stations used in 1981, depth contours of hypocenters in the Benioff zone, and reliably located earthquakes with depths less than 60 km. Station locations are indicated by solid triangles and their abbreviations. Thick dashed lines outline the contours of the Benioff zone in 10 km depth intervals [adapted from Grange et al., 1984]. Solid circles show events whose epicenters and depths are uncertain by less than 7 km (as estimated by Grange et al. [1984]), while open circles show events with epicenters and depths uncertain by less than 15 km.

Universidad de San Agustin in Arequipa.) A total of 20 sites were occupied during the investigation (three of the sites were very close to station CAB, so only the location of CAB is plotted in Figure 2).

Details of the initial data reduction procedure are given elsewhere [Grange et al., 1984; hereafter referred to as G84], as is the procedure used for determining and testing earthquake locations. The error in P arrival readings was estimated by G84 to be less than 0.1 s, while S arrivals could be uncertain by 0.8 s. The precision of the 592 best hypocentral locations was estimated to be 7 km in depth and 5 km in epicentral coordinates for intermediate depth events and 5 and 3 km, respectively, for shallow events.

In selecting a data set to use in the determination of the three-dimensional velocity structures, we first tried to see if significant improvement could be made in the locations by using a more sophisticated velocity structure. G84 had used a combination of three one-dimensional models to mimic a two-dimensional model, based on the work of previous investigators [Couch et al., 1981; Ocola et al., 1971; James, 1971], of a crust that thickens from about 12 km beneath the ocean to 70 km beneath the Altiplano. Using a location algorithm that employs an approximate ray tracing technique similar to that described by Thurber and Ellsworth [1980], we were able to locate the events with a model that more closely resembles those inferred by the investigators cited above In addition, some investigators had determined the existence of low-velocity zones (LVZ's) for shear waves both within the continental crust [Ocola and Meyer, 1972] and within the mantle beneath the oceanic crust [James, 1971]. We searched for possible shear wave LVZ's by constructing plots of P travel time versus S-P travel time (Wadati plots) for events in different depth ranges (Figure 3). The ratios of P to S velocity (V_P/V_S) deduced from these plots reveal no large-scale (>30-km dimension) shear wave LVZ under the array to depths of 100 km. Between 100 and 130 km, however, a value of 1.76 ± 0.01 was determined for V_P/V_S. Since this value represents an average of V_P/V_S from the surface to 130-km depth, and since arrivals from earthquakes in the upper 100 km yield values of 1.74 ± 0.01, the V_P/V_S between 100- and 130-km depth could be as high as 1.84, suggesting the existence of low shear wave velocities in this depth range.

The model used to relocate the events (Figure 4) is divided into a series of rectangular prisms, within each of which the velocity is presumed constant. Values for P and S velocities were derived both from the works cited above and from the V_P/V_S ratios determined from the Wadati plots. All of the 1100 earthquakes initially located by G84 were relocated with this model. In

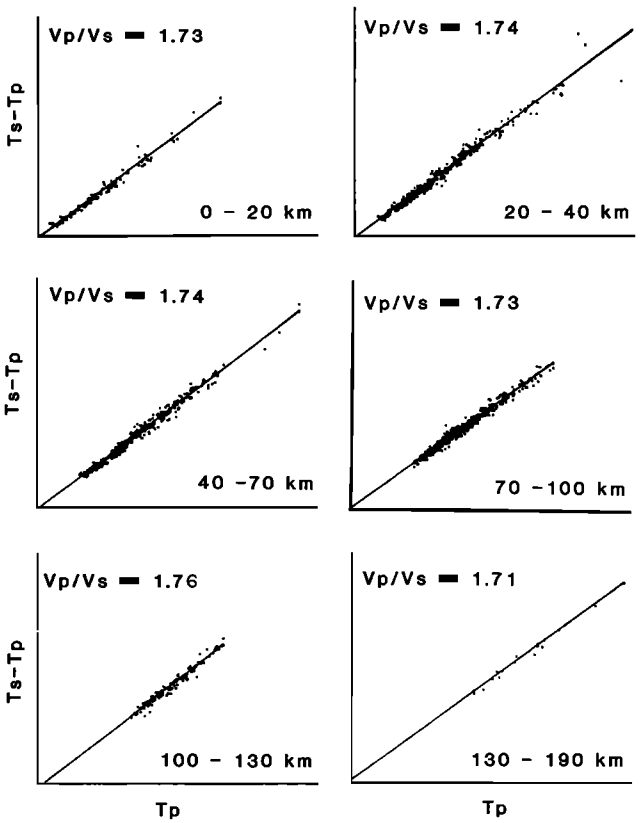

Fig. 3. Plots of P travel time (Tp) versus S-P travel time (Ts - Tp) for arrivals from events in different depth ranges. The value of V_P/V_S deduced from these plots is given in the upper left corner of each plot. The standard error in each of the determinations is about ±0.01.

selecting the best locations from this relocated set, we applied the same criteria as G84, with two additional qualifications that have bearing on the use of the data in a velocity inversion. First, the upper limit on the condition number (i.e., the ratio of largest to smallest singular values) of the matrix of hypocenter partial derivatives was taken to be 100. Second, the iterative procedure used to locate the events was required to converge; locations oscillating by more than 2 km during the final iteration were removed. Of the initial 1100 events, 442 satisfied all of these criteria. We then decided to relax the original root-mean-square (rms) residual requirement of G84, since some of the misfit in the data could be due to improper modelling. The revised rms residual rule was (1) if the number of recorded phases (N) is less than 15, the rms residual must be less than 0.5 s, (2) if $15 \leq N \leq 20$, the rms residual must be less than 0.6 s, and (3) if $N > 20$, the rms residual must be less than 0.7 s. An additional 100 events were included in the selected data set after this rule was applied.

No significant change was found in the locations as a result of the incorporation of the more sophisticated model. Differences in depth and epicenter were generally less than 7 and 5 km, respectively, and origin times were generally different by 0.5 to 1.0 s. Of the 542 events that passed all of the criteria described above, 499 were among those selected as best by G84. This agreement in event selection is not surprising, since G84 had performed tests on the effects of laterally varying structure on the earthquake locations as part of the selection procedure. At the same time, the rms residual values decreased as a result of relocation by about 0.1 s on average, indicating that the more sophisticated model is closer to reality.

The spatial distribution of selected events is an important consideration in performing a velocity inversion. The presence of a subducted slab beneath the array allows a fairly continuous distribution of events from the near-surface to about 160-km depth. In addition, a zone of events with depths less than 60 km extends from the slab to the surface near the eastern edge of the coastal plains (Figure 2). The broad distribution of event depths and epicenters and the wide aperture of the seismograph array ensures a wide variety of ray directions throughout the region, which in turn decreases the affects of coupling and anisotropy on the deduced velocity structures.

Method

The three-dimensional velocity structures discussed in this paper are arrived at through minimizing, in a damped least squares sense, travel time residuals of P and S waves from locally recorded earthquakes by adjusting simultaneously the velocities in a discretized model of the earth and the hypocentral coordinates of the earthquakes used. The method is a modification of the "block" inversion scheme originally proposed by Aki and Lee [1976]. Most of the procedures used have been described in detail elsewhere [Roecker, 1982]. Therefore only a brief review will be given here.

The three-dimensional structure is parameterized by a set of layers bounded by horizontal interfaces, each of which is divided into a mesh of rectangular prisms by two orthogonal sets of vertical interfaces. The P and S wave velocity within each block is specified independently, and each arrival time is treated as an independent observation. Perturbations to these velocities, along with adjustments to hypocentral coordinates, are determined simultaneously. Differences in station elevations are accounted for, and station corrections are not applied, as any consistent offset in arrival time at a given station is presumed to be due to local structure. The parameter separation technique [Pavlis and Booker, 1980] is employed so that a large number of events can be used without exceeding the storage space available on the computer. Stochastic damping is performed by adding a constant to the diagonals of the matrix of normal equations [e.g., Aki and Lee, 1976]. Partial derivatives of travel time with respect to the hypocenter or velocity parameters are weighted to reflect the expected accuracy of the observation. Generally, S wave residuals are given half the weight of P wave residuals.

The principle difference between the three-dimensional inversion method used here and that used by Roecker [1982] is our introduction of a version of an approximate ray tracing technique similar to that used by other investigators [e.g., Thurber, 1983; Horie, 1983]. Because this technique provides a reasonable estimate of travel time through a laterally varying structure, it allows the three-dimensional inversion to be iterative. Therefore possible biases in the results introduced by nonlinearity and choice of starting model are reduced, and the resulting variance in the residuals can be more realistically assessed.

A damping constant of 75 was added to the diagonals for the first two iterations, after which it was lowered to 25. Approximately 85% of the diagonal elements are more than an order of magnitude greater than the damping constant, so the damping may be considered small for most of the variables. In the interest of saving computation time, only blocks with 20 or more hits were included in the inversion. This step eliminated most of the poorly sampled blocks at the edge of the model, the perturbations to which would have been poorly resolved.

A priori information about the velocity structure of southern Peru was incorporated in the relocation and selection of events, and therefore the starting model for the three-dimensional inversion varies in two dimensions (Figure 4). Perturbations to this initial structure are deduced by a two-step iterative procedure. First, the earthquakes are located in the assumed two-dimensional structure or, later, in a deduced three-dimensional structure. Second, this structure is perturbed. These two steps are performed iteratively until there is no significant reduction in the residual variance.

As a result of a given iterative step in a three-dimensional velocity inversion, the velocities in some of the blocks may not be perturbed because of insufficient data, and others may be perturbed too much because of poor

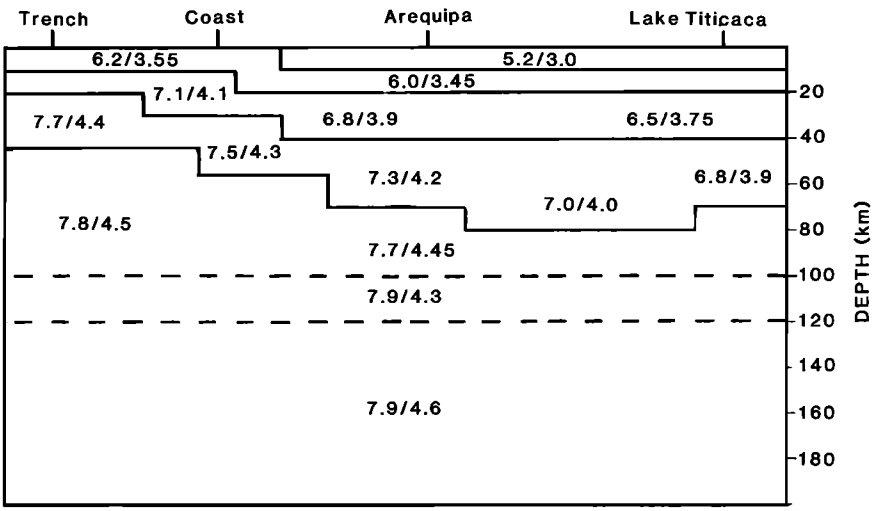

Fig. 4. Schematic representation of the two-dimensional model used both to initially relocate events and as a starting model for the three-dimensional inversions. P and S wave velocities are given in kilometers per second. Values shown are averages in their respective areas, as velocities between vertical boundaries grade laterally.

resolution, nonlinearity, or improper parameterization. To reduce possible instability caused by these effects, the structures are smoothed from one iteration to the next. For unadjusted blocks this is done by assigning an average velocity calculated from the velocities in surrounding blocks. Smoothing in adjusted blocks is accomplished by damping those perturbations that exceed one standard deviation of the perturbations in a given layer. The amount of damping is weighted by the resolution associated with the perturbation, so that large, well-resolved perturbations may not be smoothed. Note that smoothing is done only on intermediate steps. The results from the final iteration quoted in this paper have not been smoothed.

Results

Model Specifications

Discretizing the earth by dividing it into a mesh of rectangular prisms may introduce some bias into the deduced structures because in most cases the positions of the interfaces between the prisms do not correspond to those of any real discontinuities in the earth. Moreover, since these interface positions are not adjusted as part of the iterative procedure, the influence of a particular choice of discrete model may not be apparent in the usual indicators of least squares solution quality (e.g., resolution and covariance). Optimally, the velocity perturbation deduced in a prism represents an average over the whole volume. However, some misrepresentation of structure may result from spatial aliasing or inadequate data sampling. In applying this inversion technique therefore it is necessary to perform a series of inversions with different interface positions to test for any effects of improper modeling. Several models were tried during the course of this investigation, and the results of most of these inversions are given in detail elsewhere [Cunningham, 1984]. Accordingly, only a brief description of these tests will be given here.

In each inversion the starting model was adopted from the one used to initially relocate the earthquakes (Figure 4). Of course, a given set of interfaces may not line up with those assumed for initially relocating the earthquakes. In those cases, average velocities were assigned to blocks that encompassed regions of different initial velocities. The orientation of the blocks was always assumed parallel to the coast, since the trench and most of the prominent geological features on the continent are oriented in this direction (Figure 1). Block sizes were chosen by observing the number of ray paths or "hits" in a volume, as well as the size of the associated diagonal of the matrix of normal equations. More densely sampled volumes (typically those with more than 300 hits), usually located in the center of the mesh, were subdivided into smaller blocks.

The boundaries in the first starting model (model 1; Table 1) were chosen to coincide as closely as possible with those of the relocation model. Three alternate models were formed by displacing the horizontal boundaries by 10 km up and down (models 2 and 3, respectively) and by shifting the vertical interfaces parallel to the coast inland by a distance of half a block in the northeast direction (model 4). Besides revealing any unsuspected small-scale anomaly that may be misrepresented by spatial aliasing, the major purpose behind trying these alternate models was to see if a better estimate of the depth and dip of the Mohorovicic discontinuity (Moho) could be made. All four models reduced the variance in the residuals by about the same amount (≈60%, or ≈40% reduction in standard deviation, after two iterations). Model 4 gave essentially the same results as model 1, but there was a significant difference between the results of model 1 and models 2 and 3; namely, that the increases in velocity beneath the continent across the interface at 70-km depth in model 1 (e.g., 6.7 to 8.0 km/s; Figure 5) were usually much higher than

TABLE 1. Specifications for the Interface Configuration of Model 1

Layer	Depth km		Interface Position 1	2	3	4	5	6	7	8	9	10	11
1	0.	NS	-165.0	-75.0	-27.0	0.0	38.0	65.0	165.0				
		EW	-220.0	-120.0	-70.0	-10.0	14.0	55.0	110.0	220.0			
2	5.	NS	-165.0	-82.5	-55.0	-27.5	0.0	27.5	55.0	165.0			
		EW	-220.0	-110.0	-88.0	-66.0	-44.0	-22.0	0.0	22.0	44.0	82.5	220.0
3	20.	NS	-165.0	-82.5	-55.0	-27.5	0.0	27.5	55.0	165.0			
		EW	-220.0	-110.0	-88.0	-66.0	-44.0	-22.0	0.0	22.0	44.0	82.5	220.0
4	40.	NS	-165.0	-82.5	-55.0	-27.5	0.0	27.5	55.0	165.0			
		EW	-220.0	-110.0	-88.0	-66.0	-44.0	-22.0	0.0	27.5	82.5	220.0	
5	70.	NS	-165.0	-82.5	-55.0	-27.5	0.0	27.5	55.0	165.0			
		EW	-220.0	-110.0	-88.0	-66.0	-44.0	-22.0	0.0	27.5	82.5	220.0	
6	100.	NS	-165.0	-82.5	-55.0	-27.5	0.0	27.5	55.0	165.0			
		EW	-220.0	-110.0	-88.0	-66.0	-44.0	-22.0	0.0	27.5	82.5	220.0	
7	130.	NS	-165.0	-82.5	-55.0	0.0	55.0	165.0					
		EW	-220.0	-110.0	-55.0	0.0	55.0	110.0	220.0				
8	160.	NS	-165.0	-55.0	55.0	165.0							
		EW	-220.0	-110.0	0.0	110.0	220.0						
9	190.	NS	-165.0	-55.0	55.0	165.0							
		EW	-220.0	-110.0	0.0	110.0	220.0						

The interface postions are distances in kilometers from the center of coordinates, which is at 16°S 72°W. East and south are positive directions. The interface orientations (NS and EW) are rotated 62.5° west of north.

those across the interfaces at 60- and 80-km depth in models 2 and 3, respectively. Because the velocity within a block optimally represents an average of the true (perhaps varying) velocities, and because these velocities are in the range of those expected for a continental crust and upper mantle, this result suggests that 70 km is a reasonable estimate for the depth of the Moho underneath the continent. In what follows, we will concentrate on the results of the inversion using model 1.

A comment should be made on the format used to present these results (Figures 5-7). Strictly speaking, the velocity that is determined in a block should be the average for the earth within that volume, and we have no information about how velocity varies within a block. However, if we assume that the velocity in the earth is smoothly varying, we can draw contours that depict gradients of velocity between blocks. While not entirely correct, these contours make the variations in velocity easier to visualize, and so we chose to use them in presenting the results and in inferring correlations with geographic features. The positions of the blocks are plotted in Figure 6, and the values from which these plots are generated are given in Figure 5, so that readers can evaluate the effects of contouring for themselves. All of the velocities deduced by the inversion procedure were incorporated into the figures regardless of their apparent reliability (as may be inferred from the diagonals of the resolution and covariance matrices; Figure 5) because the increase in standard error and the deterioration of reliability follow a simple pattern. Generally speaking, velocity estimates are less reliable toward the edges of the array, especially toward the northeastern edge. Furthermore, velocity estimates at depths shallower than 100 km are more reliable than those deeper than 100 km.

Based on a comparison of results of runs with different models and results of different iterations using the same model, we estimate an error in the more reliable results of ±0.1 km/s, which is about the same size as the standard error deduced from the diagonals of the covariance matrix.

Results of Model 1

The earth model used in model 1 was composed of nine layers (Table 1) with the deepest interface at 190-km depth. Given the distribution of events, however, structure beneath most of the array could be resolved only to depths of about 130 km. The results discussed here are those obtained after four iterations, although most of the features discussed below, as well as most of the reduction in data variance (≈60%), resulted from adjustments made as a result of the first iteration, which suggests that the inverse problem was fairly linear. The trends in velocity deduced from the P and S solutions are generally the same, with a few discrepancies that are discussed below. This similarity in results lends credence to the structures deduced and shows that there was little trade-off between the solutions for the two structures.

The first layer is thin (5 km thick) and contains no events (Figure 6). The primary purpose of including this thin layer was to absorb any systematic travel time residuals due to local geology or to timing offsets at any station. Accordingly, the positions of the vertical interfaces in this layer were chosen so that each station lay in a separate block. The results for both P and S velocity structure show regions of high velocity along the coast and inland, alternating with regions of low velocity. We note that the stations located in the high-velocity regions are situated on or near the

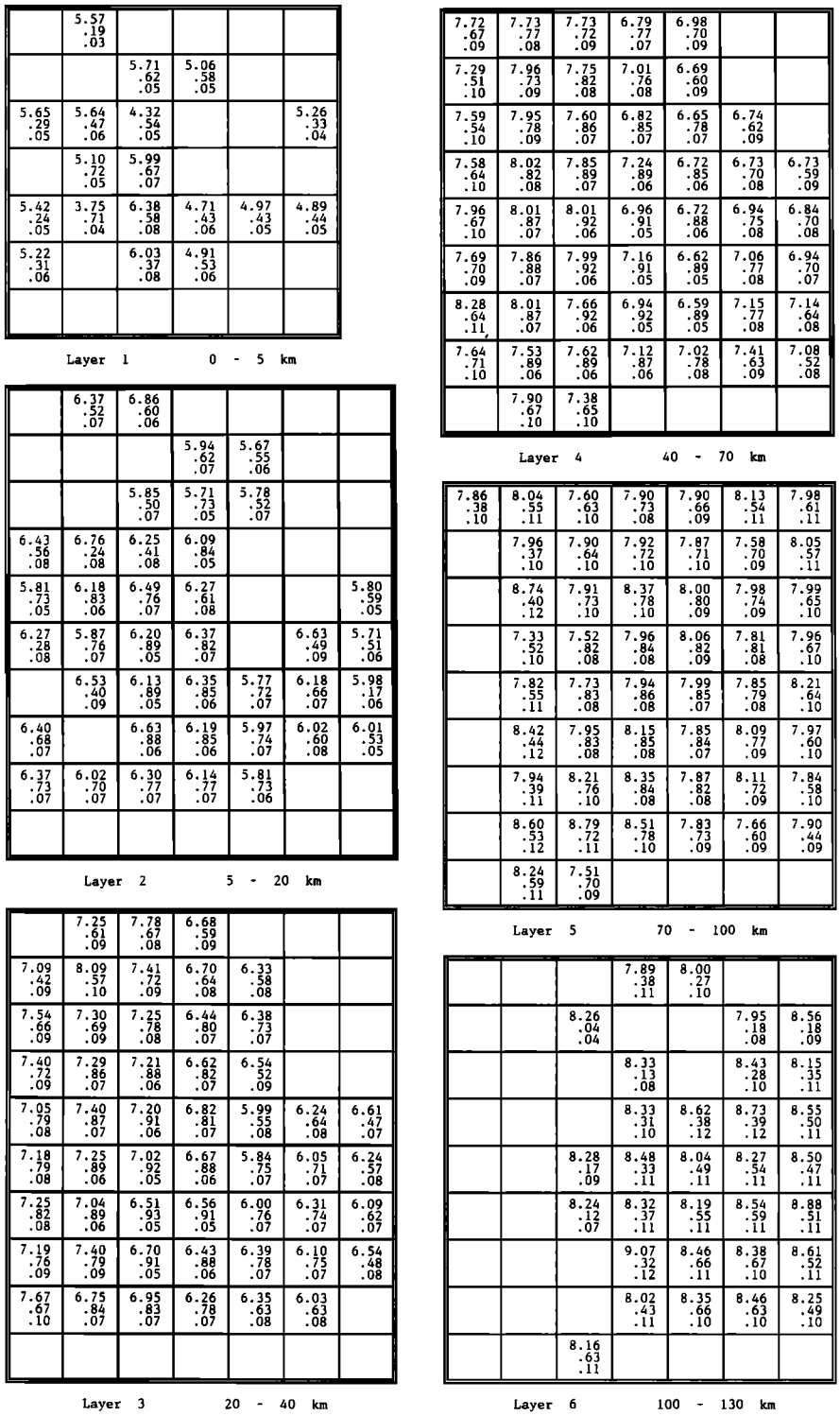

Fig. 5a

Fig. 5. Results of the inversion using model 1 (Table 1). Numbers in each box are the velocity in kilometers per second, the diagonal of the resolution matrix, and the standard error in kilometers per second determined from the diagonal of the covariance matrix and the standard deviation in the travel time residuals. The top row of boxes in each layer corresponds to the northeasternmost boxes in Figure 6. (a) Results for P wave structure in layers 1-6. (b) Results for S wave structure in layers 1-6. (c) Results for P (left) and S (right) wave structure in layers 7-9.

	3.48 .19 .02				
		3.24 .72 .03	2.74 .64 .03		
3.59 .49 .04	3.53 .59 .04	3.08 .54 .04			2.99 .40 .03
	3.15 .76 .03	3.41 .76 .04			
3.53 .29 .04	2.88 .68 .04	3.75 .68 .05	2.97 .50 .03	3.26 .30 .03	2.82 .50 .03
3.14 .37 .04		3.66 .37 .05	2.73 .64 .03		

Layer 1 0 - 5 km

	3.65 .58 .04	3.79 .64 .03				
			3.65 .63 .04	3.35 .48 .04		
		3.58 .65 .04	3.52 .73 .04			
4.04 .59 .05	4.13 .32 .05	3.56 .68 .05	3.53 .86 .03			
3.56 .75 .04	3.78 .86 .03	3.77 .82 .04	3.63 .70 .04			3.20 .61 .03
3.47 .54 .05	3.40 .86 .03	3.69 .91 .03	3.79 .85 .04			
	3.59 .65 .05	3.57 .92 .03	3.63 .89 .03	3.50 .68 04	3.23 59 .04	
3.90 .70 .04	3.76 .55 .05	3.67 .92 .03	3.46 .87 .03	3.44 .73 .04	3.43 .50 .04	3.33 .49 .03
3.86 .77 .04	3.64 .76 .04	3.51 .84 03	3.56 .79 .04	3.88 .66 .05		

Layer 2 5 - 20 km

	4.39 .67 .05	4.52 .72 .05	4.31 .61 .06			
4.07 .49 .05	4.51 .65 .06	4.19 .76 .05	4.02 .66 .05			
4.09 .69 .05	3.99 .75 .04	4.19 .79 .05	3.67 .80 .04			
3.92 .76 .04	4.00 .87 .03	4.11 .90 .03	3.68 .83 .04			
3.88 .79 .04	4.25 .89 .04	4.08 .92 .03	3.83 .83 .04	3.77 .49 .05		3.56 .51 .04
3.96 .83 .04	4.26 .90 .03	4.02 .94 .03	3.82 .90 .03	3.54 .76 .04		
4.01 .82 .04	4.02 .91 .03	3.85 .94 .03	3.83 .92 .03	3.63 .80 .04	3.63 .66 .05	3.86 .49 .05
4.11 .80 .05	4.23 .83 .05	3.86 .93 .03	4.00 87 .04	4.10 .72 .05	3.66 .69 .04	3.98 .39 .05
3.89 .70 .05	3.87 .83 .04	3.98 .87 .04	3.71 .80 .04	3.78 .65 .05		

Layer 3 20 - 40 km

4.48 .65 .05	4.51 .77 .05	4.59 .74 .05	3.91 .78 .04	4.16 .63 .05		
4.17 .54 .05	4.62 .74 .05	4.55 .84 .04	3.97 .79 .04			
4.44 .57 .06	4.56 .80 .05	4.44 .87 .04	4.10 .85 .04	3.88 .69 .05		
4.20 .65 .05	4.52 .86 .04	4.45 .92 .03	4.21 .89 .04	3.84 .81 .04		
4.43 .72 .05	4.64 .89 .04	4.65 .93 .03	4.18 .91 .03	3.96 .88 .03		4.05 .66 .05
4.32 .71 .05	4.51 .90 .04	4.65 .93 .03	4.24 .92 .03	4.05 .86 .04	3.89 .66 .05	3.89 .71 .04
4.36 .68 .06	4.54 .88 .04	4.37 .94 .03	4.10 .92 .03	3.88 .87 .04	4.21 .64 .05	3.98 .67 .05
4.25 .75 .05	4.40 .89 .04	4.36 .90 .04	4.09 .87 .04	4.03 .72 .05		
	4.38 .64 .06	3.90 .69 .05				

Layer 4 40 - 70 km

4.27 .37 .05	4.57 .55 .06	4.39 .68 .05	4.65 .68 .06	4.56 .63 .06	4.39 .50 .06	
	4.44 .43 .06	4.38 .68 .05	4.58 .70 .06	4.66 .66 .06	4.15 .65 .05	4.44 .47 .06
	4.92 .46 .07	4.52 .74 .05	4.73 .78 .05	4.60 .74 .06	4.68 .66 .06	4.38 .58 .06
	4.54 .51 .06	4.32 .83 .05	4.55 .84 .05	4.46 .77 .05	4.28 .78 .05	4.35 .63 .06
	4.71 .60 .06	4.50 .84 .04	4.53 .86 .04	4.51 .82 .05	4.38 .74 .05	4.41 .66 .05
	4.68 .57 .06	4.49 .85 .04	4.67 .85 .05	4.17 .82 .04	4.42 .79 .05	4.68 .57 .06
	4.47 .49 .06	4.60 .80 .05	4.82 .83 .05	4.27 .81 .04	4.13 .69 .05	
	4.76 .58 .07	4.90 .72 .06	4.91 .80 .05	4.19 .70 .05	4.19 .60 .06	
		4.27 .64 .06				

Layer 5 70 - 100 km

			5.00 .33 .06	4.49 .20 .05		
		4.65 .06 .03			4.97 .20 .05	4.56 .19 .05
					4.96 .27 .06	4.73 .29 .06
			4.57 .41 .06	5.14 .33 .06	4.79 .41 .07	4.97 .50 .07
		4.71 .26 .06	4.64 .40 .06	4.72 .45 .06	4.49 .49 .06	4.59 .46 .06
		4.82 .20 .05	4.48 .42 .06	4.42 .59 .06	4.72 .52 .07	4.62 .49 .06
			5.05 .38 .07	4.63 .67 .06	5.00 .58 .07	4.74 .55 .06
			4.64 .50 .06	4.47 .69 .05	4.53 .63 .06	
		4.64 .66 .06				

Layer 6 100 - 130 km

Fig. 5b

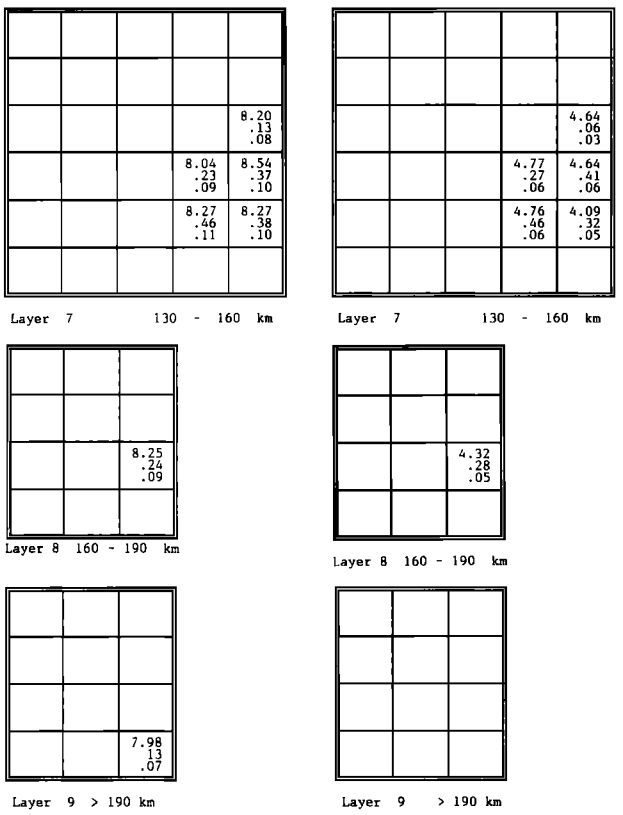

Fig. 5c

exposed Precambrian basement of the Arequipa massif, both along the coast (SGP, MOL, and AYE) and at the eastern edge of the coastal plains (ARE, LLU, RAT, and CAY). The stations in the intervening low-velocity region (TOR, SIS, CAN, and ONG) all sit on Quaternary alluvium. The low velocities to the northeast are associated with stations located at high elevation within the Cordillera Occidental. This apparent correlation between the surface geology and velocity structure at shallow depths suggests that the average residuals at each station are due to local structural variations in the upper few kilometers, rather than being caused by any timing errors.

The structure in layer 2 (5- to 20-km depth) generally shows the velocities in the southwest to be higher than those in the northeast, although the boundary between the two is complicated. There is also a prominent low situated in the middle of the high-velocity zone at about 16.5°S and 72.5°W. We note that almost all of the earthquakes in this layer are located in the higher velocity regions.

Layers 3 (20- to 40-km depth) and 4 (40- to 70-km depth) reveal a large-scale zoning of high and low velocities, the highs being relegated to the southwest and the lows to the northeast. The gradient in velocity is steep in the region beneath the eastern edge of the Arequipa massif, suggesting that a real discontinuity, probably the Moho, is situated here. This result is perhaps not surprising considering that the starting model assumed the Moho to be located in this area. Nevertheless, the assumed two-dimensional structure of the Moho is not preserved. In both layers the velocity gradient is considerably steeper in the northwest than in the southeast.

In layer 5 (70- to 100-km depth) the northeast-southwest zonation of highs and lows has largely disappeared for P waves but persists for S waves. However, there is still a steep gradient in both P and S wave velocities from southwest to northeast in the southeastern part of the array. The seismicity in the northwestern part of the array in this depth range is within the nearly horizontal slab in this area. P wave velocities exhibit a considerable amount of lateral variation near the transition region between the horizontally dipping and normally dipping slabs, with a relative high positioned at the northwest edge of the transition. A P wave velocity low located to the southeast of this high is lower than the velocity directly above it in layer 4 and thus represents an inversion in velocity with depth. This low continues into layer 6 (100-130 km) although displaced somewhat to the northeast. S wave velocities in these layers mimic the P wave trends, although with less contrast.

At depths greater than 100 km (layers 6-9), resolution falls off (Figure 5), so that with the exception of the southeastern part of layer 6, the velocity perturbations tend to trade off with other blocks or with hypocenter locations and hence are less reliable. Therefore the results in layers 7-9 were not contoured. We note that the positions of the vertical interfaces in layer 6 were initially the same as those in layer 7 (130- to 160-km depth; Figure 6, Table 1). In an attempt to resolve additional structure in the upper mantle, the interfaces in layer 6 were changed to be the same as those in layer 5 after the second iteration. This change altered the structure deduced in layer 6 only slightly and had no effect on the structure determined in the upper layers.

The deviation of the lower crust from a two-dimensional structure may be better viewed by comparing cross sections perpendicular to the structural trends (Figure 7). These sections reveal the gradual, nearly monotonic decrease in the northeast-southwest velocity gradient from the northwest to the southeast that was suggested in the map views (section 5 is an exception; Figure 8). Again, because the velocities determined are averages over the volume of a block, we cannot say whether or not these gradients represent an actual discontinuity and, moreover, whether or not the change in gradient represents a change in dip in the discontinuity or merely a difference in change in velocity across it. Our prejudice is that a real discontinuity in this area seems likely, and therefore we will assume in the discussion that these changes in gradient reflect a change in the dip of the Moho.

As may be expected, the P and S wave velocities within the slab (as defined by the microearthquake locations) are typically higher than those in the surrounding mantle. In addition, the top of the slab at depths greater than 70 km appears to be roughly outlined in most of the cross sections by the 4.6-km/s S wave velocity contour. Since the dip of the slab, and hence the dip of the contours, increases to the

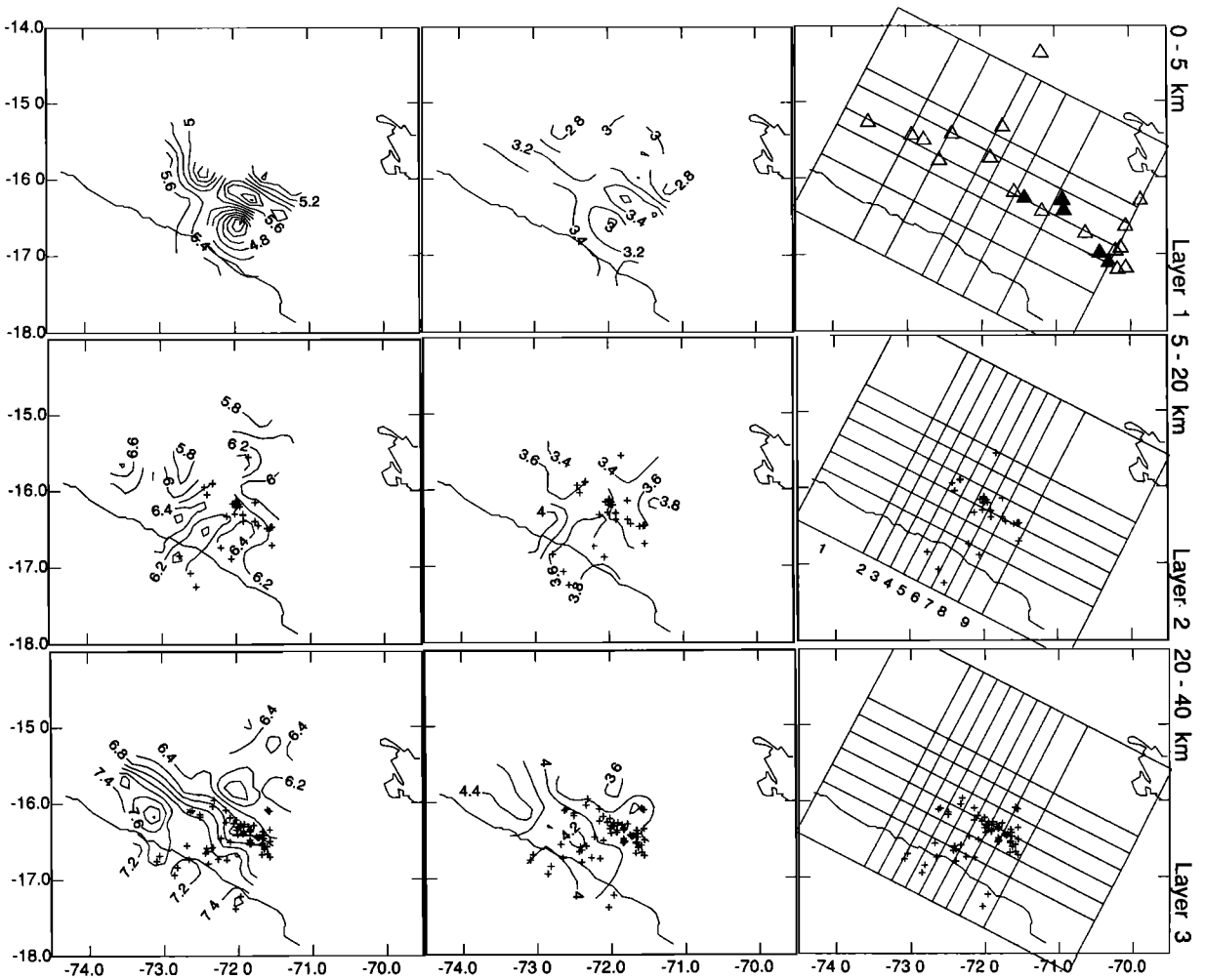

Fig. 6. Contours of the velocity structure determined from the inversion using model 1. The contour interval is 0.2 km/s. The three boxes in each row depict, from left to right, contours of P wave velocity structure, contours of S wave velocity structure, and the configuration of the interfaces in layers 1-6. Only the interface configurations for layers 7 and 8 as the velocities in layers 7-9 were not contoured (the configuration in layer 9 was the same as that in layer 8) because very few of the results in these layers were well resolved. Crosses indicate the epicenters of earthquakes located in each layer. The coastline and part of Lake Titicaca are shown in each figure for reference. The locations of active and dormant volcanoes are shown in layer 1 by solid and open triangles, respectively.

southeast, the shear wave velocities in the mantle between about 70 and 130 km are lower in the southeast than in the northwest. P wave velocities also tend to be low in some areas above the slab in the southeast, although the correlation is not as striking as it is for S waves.

One feature that does not show up well on the cross sections, due to the type of contouring routine used, is the reversal in velocity in layers 5 and 6 discussed above. These reversals are located above the top of the slab near the point where the slab begins to flatten to the northeast.

Discussion

Previous investigators [Barazangi and Isacks, 1979; Jordan et al., 1983] have pointed out correlations between the changes in the dip of the subducted Nazca plate and the tectonics of the overriding South American plate. For example, the tectonics above flat slabs are characterized by a lack of recent active magmatism, active crustal shortening in the sub-Andes, and recent uplift of the crystalline basement on high-angle reverse faults, while regions above steeply dipping slabs have an active volcanic axis, a high plateau (the Altiplano or Puna), a high Neogene but inactive thrust belt (the Eastern Cordillera), and an active eastward migrating sub-Andean thin-skinned thrust belt. Studies of seismicity [e.g., Stauder, 1975; Suarez et al., 1983] show that large thrust events are common at the western edge of the sub-Andes above the flat slab region north of 14°S, but there are few if any similar events located to the south. Therefore both present and historic deformation of the South American plate appear to be intimately related to the dip of the subducted Nazca plate.

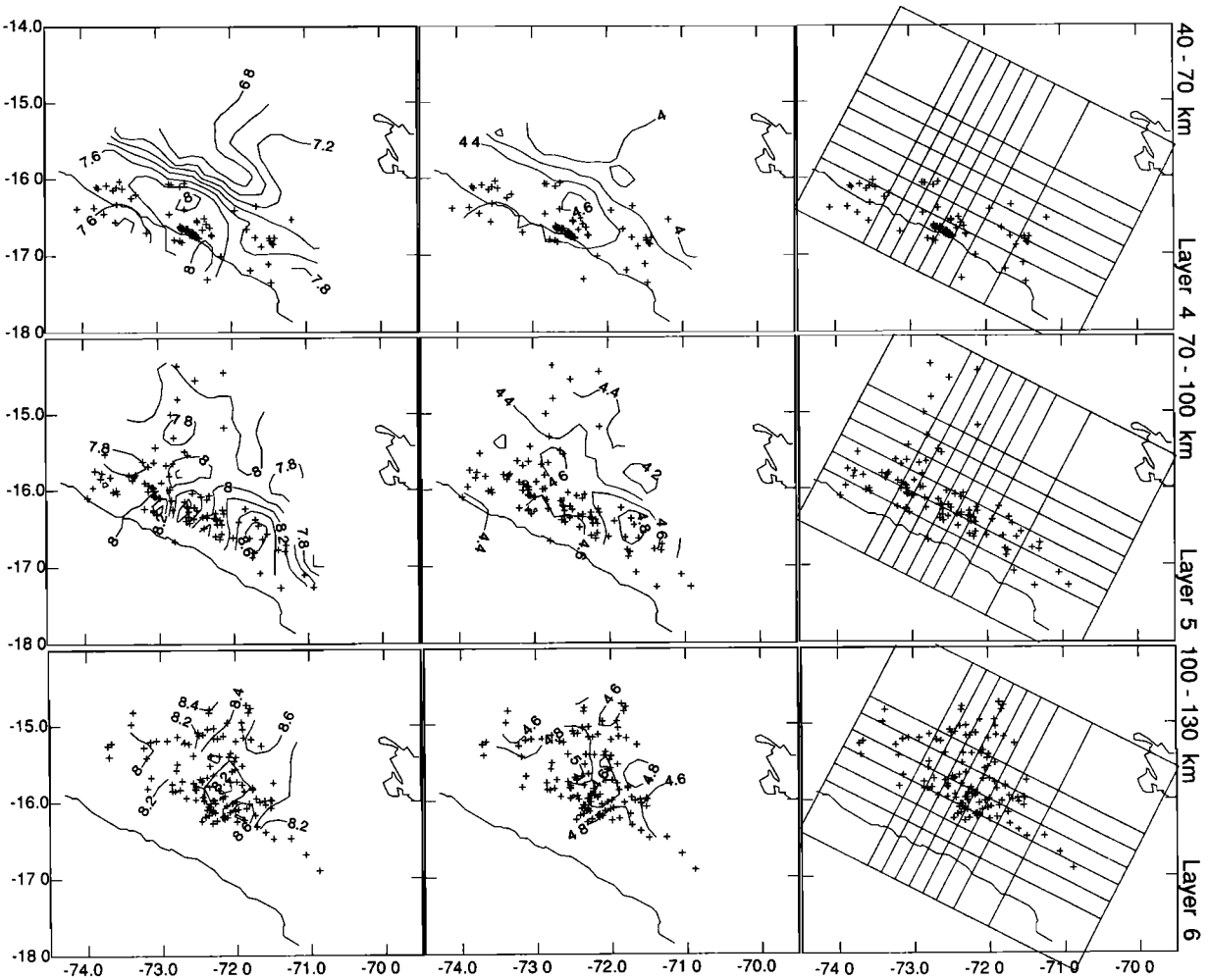

Fig. 6 (continued)

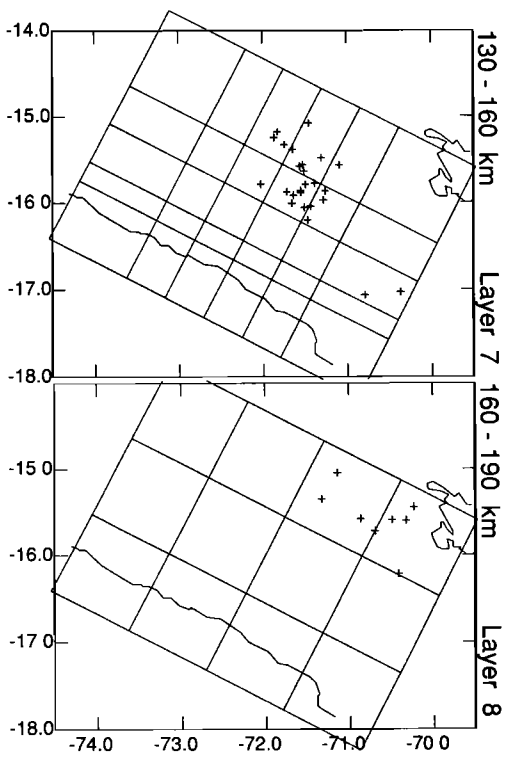

Fig. 6 (continued)

The locations of the microearthquakes used in this study clearly delineate the increasing dip of the slab from northwest to southeast (Figures 6 and 7), and several of the features of the velocity structure noted above appear to be related to this change in dip. Specifically, the inferred steeply dipping Moho is located above the flat slab segment, gradually becoming less steep over the more steeply dipping slab. Moreover, the low mantle S wave velocities between 70- and 130-km depth are apparent only above the more steeply dipping slab.

The existence of low velocities in the mantle above the steeply dipping slab corroborates the hypothesis that the lack of magmatism above the flat subducting slab is due to the lack of partially melted (and therefore lower velocity) asthenospheric material above the slab [Barazangi and Isacks, 1979]. The high value for V_P/V_S determined for this depth range from the Wadati plots (Figure 3) is most likely due to the low S wave velocities above this part of the slab.

The steepening of the dip of the Moho to the northwest is more difficult to explain in terms of previously postulated mechanics of deformation in the Andes, but the correlation of this phenomenon with the flattening of the slab suggests that the two are related. A possible explanation is that the crust above the steeply dipping Moho in the northwest represents a deformed version of the crust in the southeast.

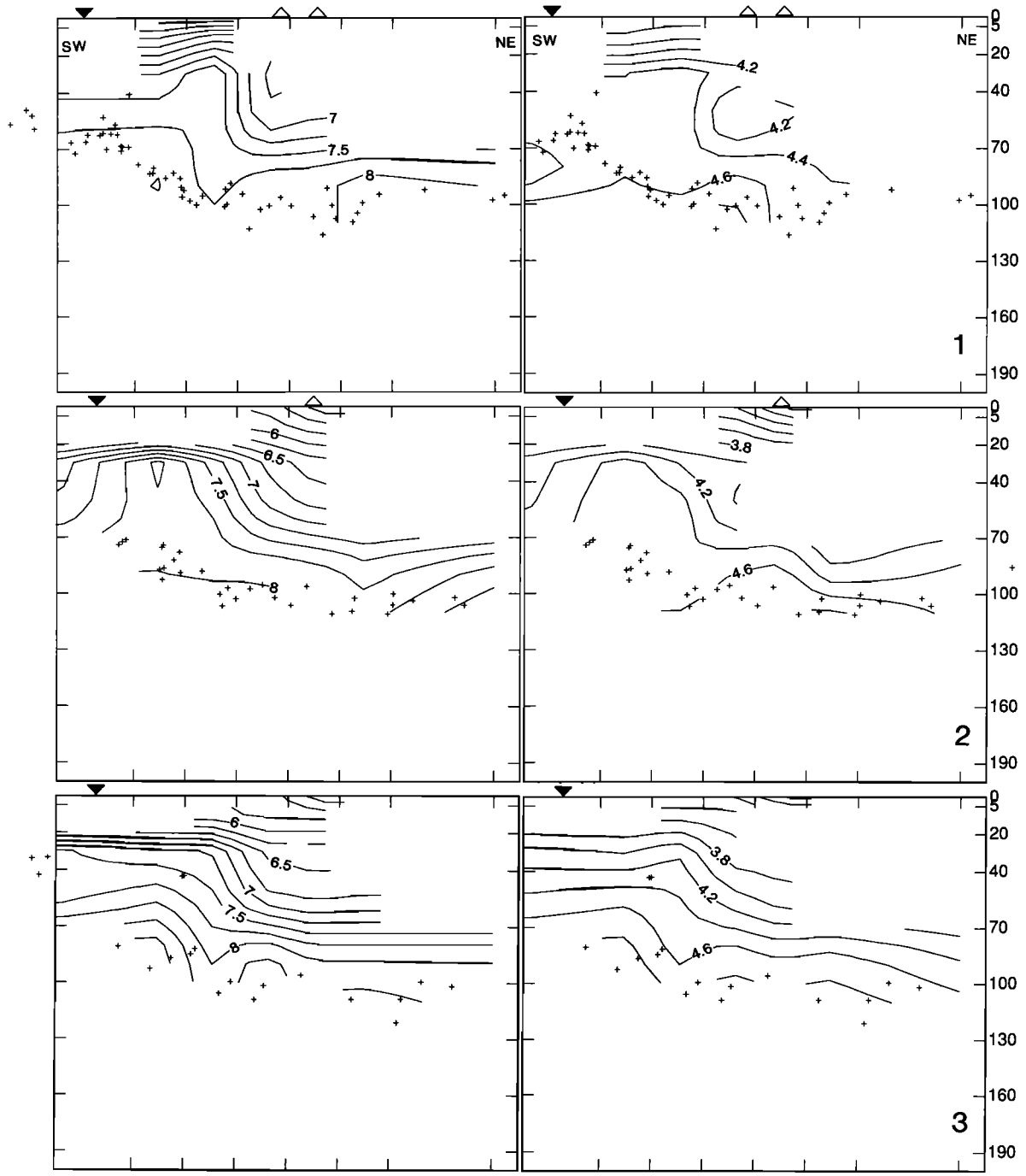

Fig. 7. Contours of velocity structure for (left) P waves and (right) S waves shown in cross section. The contour interval is 0.25 km/s for P and 0.2 km/s for S. The locations of the sections are shown on the interface map for layer 2 in Figure 6. The orientation of the sections is noted on the top of sections 1, 4, and 7. Crosses show earthquakes located in each of the sections. The depth intervals given on the right of the figure correspond to depths of layer boundaries in kilometers, while vertical tick marks indicate positions of vertical interfaces as shown in layers 2-6 in Figure 6. Vertical and horizontal scales are the same. Open and solid triangles at the top of some sections locate dormant and active volcanoes, respectively. Inverted solid triangles in each section show the location of the coast. The trench is located about 100 km to the southwest of the coast.

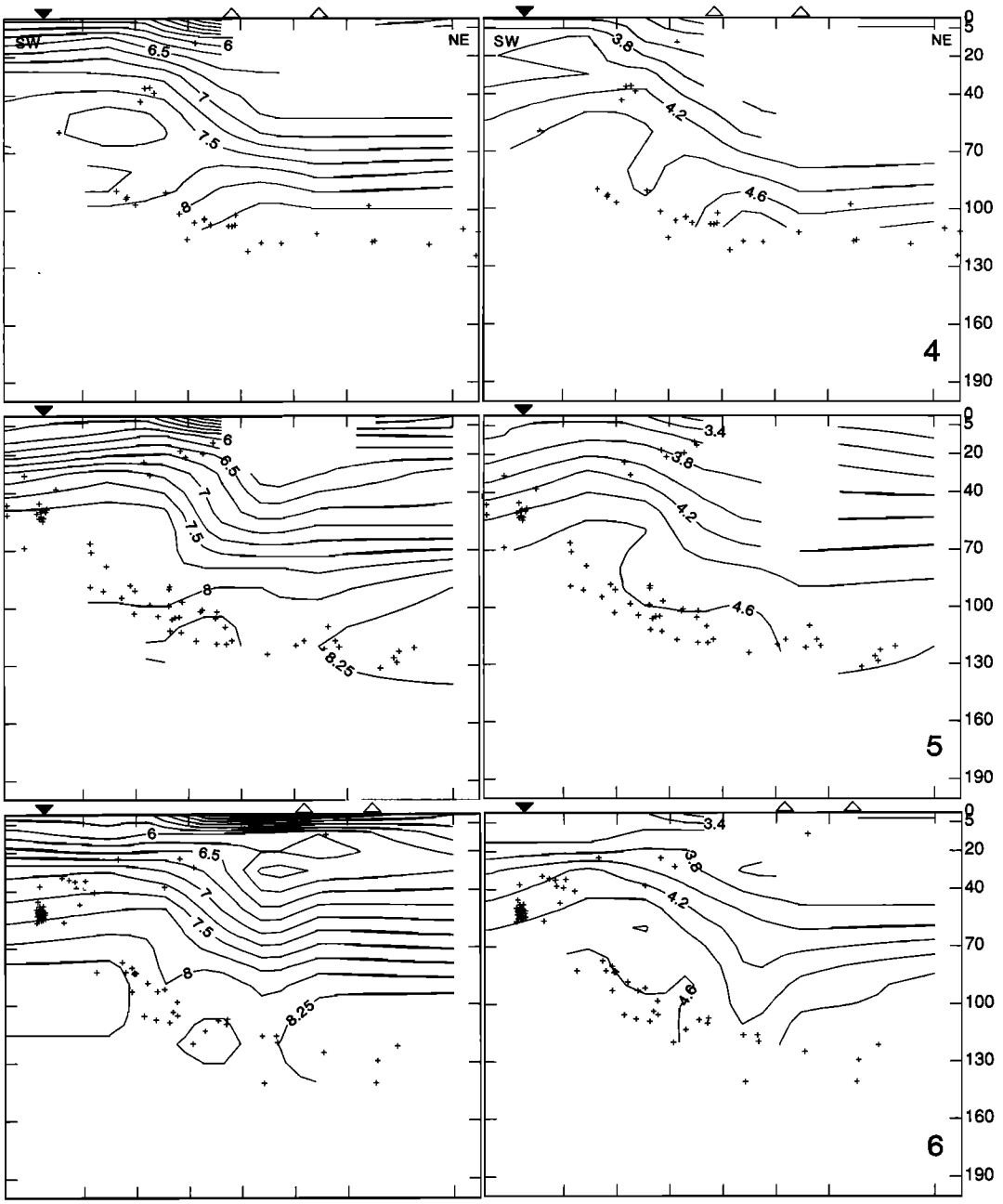

Fig. 7 (continued)

We note that there is a plane of microearthquake activity dipping westward from the surface to near the edge of the slab that occurs above the more steeply dipping slab in the southeast. These earthquakes reach the surface at a thrust fault at the contact between the Cordillera Occidental and the Arequipa massif. Owing to the breadth and dip of this zone of activity, it is tempting to interpret these earthquakes as a result of the crust beneath the Arequipa massif overthrusting the Cordillera Occidental. Indeed, if this were the case, one could postulate that the gently dipping Moho in the southeast is presently being steepened by such activity. However, this kind of motion is supported neither by the fault plane solutions of the microearthquakes, which reveal both strike-slip faulting and thrusting in a northwest-southeast direction (see Figures 4 and 5 in G84), nor by geological evidence, which while showing that west dipping thrust faults indeed exist at and near the western edge of the Cordillera Occidental, suggests that these faults have been inactive since Oligocene-Miocene time [Vicente et al., 1979]. The manner in which these earthquakes are contributing to crustal deformation is therefore unclear. At the same time, while G84 suggested that these earthquakes extend through the crust and on into the subducting slab, our results imply that they occur only within the crust. This difference arises from the inference that the Moho in this region dips more gently than the one assumed by

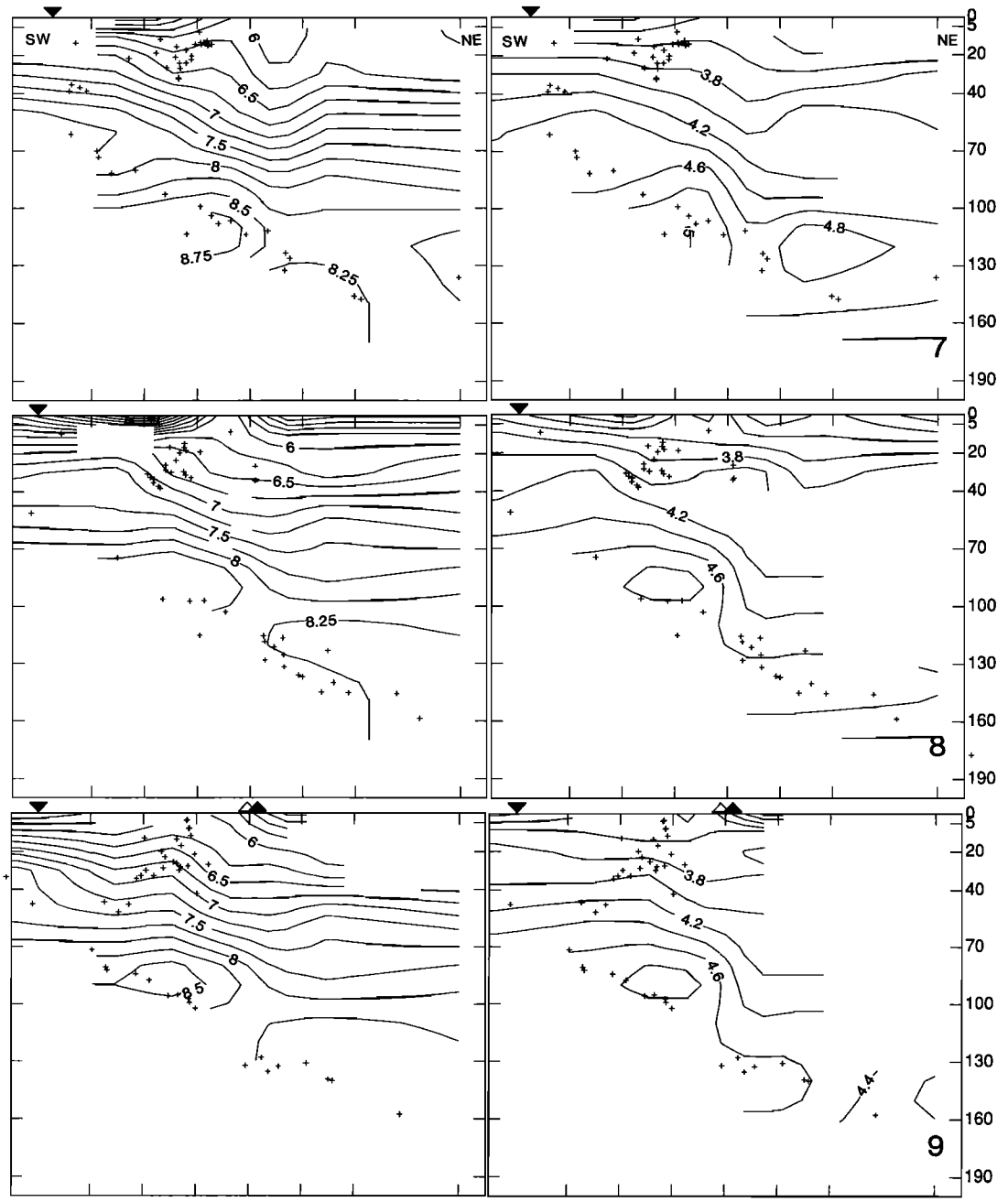

Fig. 7 (continued)

G84, which was derived from an interpretation of gravity data by Couch et al. [1981].

Most of the surface tectonic features that previous investigators found to correlate with changes in slab dip extend over a considerable distance. However, the limited spatial extent of the array used to deduce the velocity structure in southern Peru allows no inference about how the features determined in this study relate to structure in neighboring areas. In fact, a rough interpretation of the free-air gravity anomalies in the area (Figure 9) suggests that features such as the change in Moho dip exist only locally. Although the anomaly map is too complicated to afford a complete interpretation based on the results of this study, there does exist an unusual gravity high of 225 mGals in the northwest part of the array that grades to a low of -54 mGals in the southeast before returning to values in the 50- to 75-mGals range. The strong gravity high in the northwest is consistent with the inference of an elevated (high density) mantle in this area, while the lower values would correspond to a thicker (and isostatically uncompensated) crust. The gravity high does not extend very far to the northwest of the array, suggesting that the elevated mantle does not either. Incidentally, there is a striking correspondence between the pronounced gravity low in the middle of the array with the low-velocity

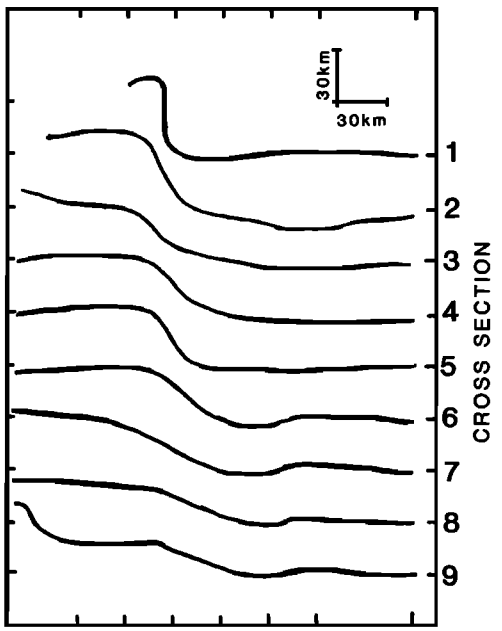

Fig. 8. Summary of the inferred change in the dip of the Moho, as indicated by the 7.5-km/s P wave velocity contour. This contour was chosen because it consistently reached the depth of 70 km beneath the Altiplano, as is indicated by the tick mark to the left of the section identifier. Vertical tick marks correspond to those plotted in Figure 7. Cross-section numbers are given in Figure 6.

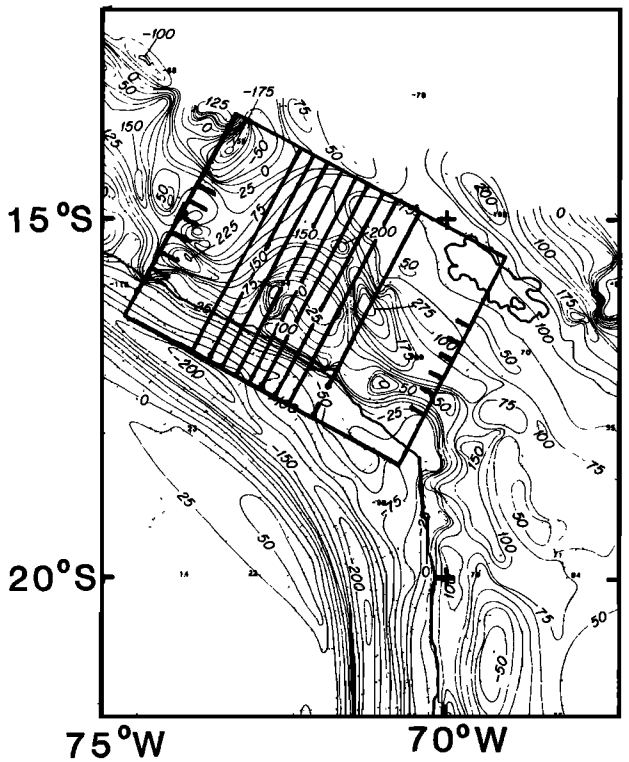

Fig. 9. Map view of the interface positions of layer 2 superimposed upon a map of the free-air gravity anomalies (in milliGals) of southern Peru. Northwest-southeast interfaces are indicated by tick marks for clarity. Gravity map adapted from Bowin et al. [1982].

region in layer 2 and with the inverted velocities in layers 5 and 6 mentioned above, all of which occur near the area were the slab changes dip. We cannot offer an interpretation of these low velocities because we do not understand the mechanics of a slab contortion well enough. Besides, the position of the low velocities does not correspond to any mapped surface feature.

While the change in the dip of the Moho determined in this study is a phenomenon that possibly does not extend far outside of the array area, it does seem to be connected with the change in the dip of the slab. The question then becomes one of cause and effect. If the steepening of the Moho is somehow caused by the flattening of the subducted slab, one can imagine that as the contortion in the slab is propagating southward, as it would if it were being caused by the oblique subduction of the Nazca ridge, the Moho to the south would steepen in the process, resulting in crustal deformation west of the Cordillera Occidental. Alternatively, if the position of the contortion is not propagating because the contortion is aligned with the direction of convergence as the results of G84 suggest, it could be that the change in Moho dip is inherited from a previous phase of deformation and could be a cause rather than an effect of the contortion in the slab.

Acknowledgments. We thank O. Ancajima, C. Anconeyra, R. Benites, A. Flores, J. Gagnepain, F. Gomez, F. Grange, J. Melgar, T. Modiano, P. Molnar, F. Pardo, A. Posadas, E. Salinas, R. Stewart, J. Stock, G. Suarez, I. Vellejos, and A. Vilkas for assistance in the field and M. Lazo, F. Megard, M. Sebrier, and J. C. Vicente for advice and help with logistics. This work was supported by NASA grant NAG5-300 of the Geodynamics Program.

References

Aki, K., and W. H. K. Lee, Determination of three-dimensional velocity anomalies under a seismic array using first P arrival times from local earthquakes, 1, A homogeneous initial model, J. Geophys. Res., 81, 4281-4339, 1976.

Audebaud, E., R. Capdevilla, B. Dalmayrac, J. Debelmas, G. Laubacher, C. Lefevre, R. Marocco, C. Martinez, M. Mattauer, F. Megard, J. Paredes, and P. Tomasi, Les traits geologiques essentiels des Andes Centrales (Perou-Bolivie), Rev. Geogr. Phys. Geol. Dyn., 15(2), 73-114, 1973.

Balley, A. W., P. L. Gordy, and G. A. Stewart, Structure, seismic data and orogenic evolution of the southern Canadian Rocky Mountains, Bull. Can. Pet. Geol., 14, 337-381, 1966.

Barazangi, M., and B. L. Isacks, Spatial distribution of earthquakes and subduction of the Nazca plate beneath South America, Geology, 4, 686-692, 1976.

Barazangi, M., and B. L. Isacks, Subduction of the Nazca plate beneath Peru: Evidence from spatial distribution of earthquakes, Geophys. J. R. Astron. Soc., 57, 537-555, 1979.

Bowin, C., W. Warsi, and J. Milligan, Free-Air Gravity Anomaly Atlas of the World, Geol. Soc. Am. Map and Chart Series, No. MC-46, 1982.

Burchfiel, B. C., and G. A. Davis, Structural

framework and evolution of the southern part of the Cordilleran orogen, western United States, Am. J. Sci., 272, 97-118, 1972.

Burchfiel, B. C., and G. A. Davis, Nature and controls of Cordilleran orogenesis, western United States: Extension of an earlier synthesis, Am. J. Sci., 275-A, 363-396, 1975.

Cobbing, E. J. and W. S. Pitcher, The coastal batholith of central Peru, Q. J. Geol. Soc. London, 128, 421-460, 1972.

Cobbing, E. J., W. S. Pitcher, and W. P. Taylor, Segments and super-units in the coastal batholith of Peru, J. Geol., 85, 625-631, 1977.

Couch, R., R. M. Whitsett, B. Huehn, and L. Briceno-Guarupe, Structure of the continental margin of Peru and Chile, Nazca Plate, Mem. Geol. Soc. Am., 154, 703-726, 1981.

Cunningham, P., Earthquake locations and three-dimensional seismic structure of southern Peru, Masters thesis, 179 pp., Mass. Inst. of Technol., Cambridge, 1984.

Dalmayrac, B., J. R. Lancelot, and A. Leyerloup, Two-billion-year granulites in the late Precambrian metamorphic basement along the southern Peruvian coast, Science, 198, 49-51, 1977.

Dalmayrac, B., G. Laubacher, and R. Marocco, Geologie des Andes Peruviennes, Caracteres generaux de l'evolution geologique des Andes Peruviennes, Travaux et Documents de l'ORSTOM, Ed. de l'Office de la Rech. Sci. et Tech. Outre-Mer, Paris, 1980.

Dewey, J. F., and J. M. Bird, Mountain belts and the new global tectonics, J. Geophys. Res., 75, 2625-2647, 1970.

Grange, F., D. Hatzfeld, P. S. Cunningham, P. Molnar, S. W. Roecker, G. Suarez, A. Rodreguez, and L. Ocola, Tectonic implications of the microearthquake seismicity and fault plane solutions in southern Peru, J. Geophys. Res., 89, 6139-6152, 1984.

Ham, C. K., and L. J. Herrera, Jr., Role of sub-Andean fault system in tectonics of eastern Peru and Ecuador, Backbone of the Americas, Am. Assoc. Pet. Geol. Mem., 2, 47-61, 1963.

Hamilton, W., The volcanic central Andes---A modern model for the Cretaceous batholiths and tectonics of western North America, Oreg. Dep. Geol. Miner. Ind. Bull., 65, 175-184, 1969.

Hasegawa, A., and I. S. Sacks, Subduction of the Nazca plate beneath Peru as determined from seismic observations, J. Geophys. Res., 86, 4971-4980, 1981.

Horie, A., Three-dimensional seismic velocity structure beneath the Kanto district by inversion of P wave arrival times, Ph.D. thesis, 59 pp., Univ. of Tokyo, 1983.

James, D. E., Andean crustal and upper mantle structure, J. Geophys. Res., 76, 3246-3271, 1971.

Jordan T. E., B. L. Isacks, R. W. Allmendinger, J. A. Brewer, V. A. Ramos, and C. J. Ando, Andean tectonics related to geometry of subducted Nazca plate, Geol. Soc. Am. Bull., 94, 341-361, 1983.

Megard, F., Etude geologique des Andes du Perou central, Mem., 86, 310 pp., Office de la Rech. Sci. et Tech. Outre-Mer, Paris, 1978.

Newell, N. D., Geology of the Lake Titicaca region, Peru and Bolivia, Geol. Soc. Am. Mem., 36, 111 pp., 1949.

Nobel, D. C., and E. J. McGee, Spatial distribution of earthquakes and subduction of the Nazca plate beneath South America: Comment, Geology, 5, 576-578, 1977.

Ocola, L. C., and R. P. Meyer, Crustal low-velocity zones under the Peru-Bolivia Altiplano, Geophys. J. R. Astron. Soc., 30, 199-209, 1972.

Ocola, L. C., R. P. Meyer, and L. T. Aldrich, Gross crustal structure under the Peru-Bolivia Altiplano, Earthquake Notes, 42, 33-48, 1971.

Pavlis, G. L., and J. R. Booker, The mixed discrete-continuous inverse problem: Application to the simultaneous determination of earthquake hypocenters and velocity structure, J. Geophys. Res., 85, 4801-4810, 1980.

Pitcher, W., On the rate of emplacement of batholiths, Q. J. Geol. Soc. London, 131, 581-591, 1975.

Price R. A., and E. W. Mountjoy, Geologic structure of the Canadian Rocky mountains between Bow and Athabaska rivers---A progress report, Geol. Assoc. Can. Spec. Pap., 6, 7-25, 1970.

Roecker, S. W., Velocity structure of the Pamir-Hindu Kush region: Possible evidence of subducted crust, J. Geophys. Res., 87, 945-959, 1982.

Sales, J. K., Cordilleran foreland deformation, Am. Assoc. Pet. Geol. Bull., 52, 2016-2044, 1968.

Stauder, W., Subduction of the Nazca plate under Peru as evidenced by focal mechanisms and by seismicity, J. Geophys. Res., 80, 1053-1064, 1975.

Stearns, D. W., Faulting and forced folding in the Rocky Mountain foreland, Laramide folding associated with basement block faulting in the western United States, Geol. Soc. Am. Mem., 151, 1-37, 1978.

Suarez, G., P. Molnar, and B. C. Burchfiel, Seismicity, fault plane solutions, depth of faulting, and active tectonics of the Andes of Peru, Ecuador, and southern Columbia, J. Geophys. Res., 88, 10403-10428, 1983.

Thurber, C. H., and W. Ellsworth, Rapid solution of ray tracing problems in heterogeneous media, Bull. Seismol. Soc. Am., 70, 1137-1148, 1980.

Thurber, C. H., Earthquake locations and three-dimensional crustal structure in the Coyote Lake area, central California, J. Geophys. Res., 88, 8226-8236, 1983.

Vicente, J. C., F. Sequeiros, M. A. Valdivia, and J. Zavala, El sobre-escurrimiento de Chincha-Lluta: Elemento del accidente mayor andino al NW de Arequipa, Bol. Soc. Geol. Peru, 61, 67-100, 1979.

P. S. Cunningham, Standard Oil Production Co., 1 Lincoln Center, 5400 LBJ Frwy., suite 1200, Dallas, TX 75240.

S. W. Roecker, Department of Geology, Rensselaer Polytechnic Institute, Troy, NY 12180.

D. Hatzfeld, Laboratoire de Geophysique Interne, Institut de Recherches Interdisciplinaires de Geologie et de Mecanique, L'Universite Scientifique et Medicale de Grenoble, France.

(Received November 15, 1985;
revised April 4, 1986;
accepted April 10, 1986.)